Gondwana Research 117 (2023) 261–273

Contents lists available at ScienceDirect

Gondwana Research

journal homepage: www.elsevier.com/locate/gr

The first dinosaurs in China: Dating Late Triassic footprint fossils from the Sichuan Basin

Shenyuan Peng [a,b], Jian Liu [c,d], Michael J. Benton [e,*], Xin Jin [a,b], Zhiqiang Shi [a,b,*]

[a] Institute of Sedimentary Geology, Chengdu University of Technology, Chengdu, Sichuan 610059, China
[b] State Key Laboratory of Oil and Gas Reservoir Geology and Exploitation, Chengdu University of Technology, Chengdu, Sichuan 610059, China
[c] Chengdu Natural History Museum, Chengdu, Sichuan 610059, China
[d] Museum of Chengdu University of Technology, Chengdu, Sichuan 610059, China
[e] School of Earth Sciences, University of Bristol, Bristol BS8 1TQ, UK

ARTICLE INFO

Article history:
Received 4 September 2022
Revised 5 January 2023
Accepted 3 February 2023
Available online 7 February 2023
Handling Editor: J. Meert

Keywords:
Late Triassic
Dinosaur footprints
Zircon U-Pb dating
Ichnotaxon
Migration
Evolution

ABSTRACT

Dinosaur footprints from the Upper Triassic Xujiahe Formation (T_3x^3) in the Sichuan Basin are the earliest records of dinosaurs from China. Hitherto, little has been known about dinosaurs from the Late Triassic of eastern Tethys and their geochronological ages. Here, we report abundant new dinosaur tracks from the Upper Triassic Tianquan track site, in Ya'an city, western Sichuan Basin. The tracks are assigned to cf. *Pengxianpus* isp., cf. *Kayentapus* isp. and elements of the *Grallator-Anchisauripus-Eubrontes* plexus based on morphospace analysis of key traits. These tracks were all produced by small theropod dinosaurs. The track-bearing beds are dated to 218.4 ± 4.7 Ma, a mid-Norian age, based on a group of the youngest detrital zircons. These earliest dinosaurs in the eastern Tethys appear to have migrated in from regions in western Tethys at similar paleolatitudes, and their movements may have been limited by substantially fluctuating paleoclimates. These theropod tracks from eastern Tethys provide additional evidence of the rise of dinosaurs to ecological dominance at a time of fluctuating paleoclimatic conditions corresponding to the mid-Norian Warming Event.

1. Introduction

The geography of dinosaur origins in the Triassic is uncertain. The oldest confirmed dinosaur skeletons come from the late Carnian (c. 230 Ma) of Argentina (upper Ischigualasto Formation) and Brazil (upper Santa Maria Formation), suggesting an origin in South America (Langer et al., 2010, 2018; Benton et al., 2018). Some sister clades of Dinosauria, including *Lagosuchus* and Lagerpetidae, probable sister clade of Pterosauria (Ezcurra et al., 2020), are also from South America, but most sister clades, such as Silesauridae and Pterosauria, have Middle and Late Triassic members from Europe and Africa (Nesbitt et al., 2010, 2013), suggesting that the early evolution of the Dinosauria, as well as their wider inclusive clades Dinosauromorpha and Avemetatarsalia, did not take place exclusively, or even mainly, in South America. Records of ichnofossils from Europe pull the origin of Dinosauromorpha down to the late Early Triassic (Olenekian, Brusatte et al., 2011).

The flourishing of dinosaurs in the mid to late Carnian may have been triggered by the Carnian Pluvial Episode (CPE), dated at 233–232 Ma, a global climatic event that triggered a major extinction and radiations in marine and terrestrial ecosystems (Bernardi et al., 2018; Benton et al., 2018; Dal Corso and Bernardi, 2020). The Late Triassic explosion of Dinosauria is marked by the broad appearance of dinosaur skeletons and footprints all over Pangaea (Fig. 1A), including southern Gondwana (South America and south Africa mainly, Marsicano and Barredo, 2004; Melchor and De Valais, 2006; Yates, 2007; Sereno, 2012; Da Rosa, 2015), northern Gondwana (North America, Olsen, 1988; Olsen and Huber, 1998; Lucas, 1998, 2010; Lagnaoui et al., 2012; Hartung et al., 2021), western Tethys (Europe, Rauhut and Hungerbühler, 2000; Klein and Lucas, 2010; Niedźwiedzki, 2011; Lallensack et al., 2017), and eastern Tethys (South China, Yang and Yang, 1987; Wang et al., 2005; Xing et al., 2013a, 2014a, b, 2018). The Late Triassic dinosaurian records from China are solely footprints, and no skeletal fossils have been found yet, leaving a substantial paleogeographic area of uncertainty (Langer et al., 2010; Benton et al., 2018; Dunne et al., 2021).

The South China Block (SCB) was initially an island, which might have prevented terrestrial animals and plants from entering

* Corresponding authors at: Institute of Sedimentary Geology, Chengdu University of Technology, Chengdu, Sichuan 610059, China (Z. Shi).
E-mail addresses: Mike.Benton@bristol.ac.uk (M.J. Benton), szqcdut@163.com (Z. Shi).

https://doi.org/10.1016/j.gr.2023.02.003
1342-937X/

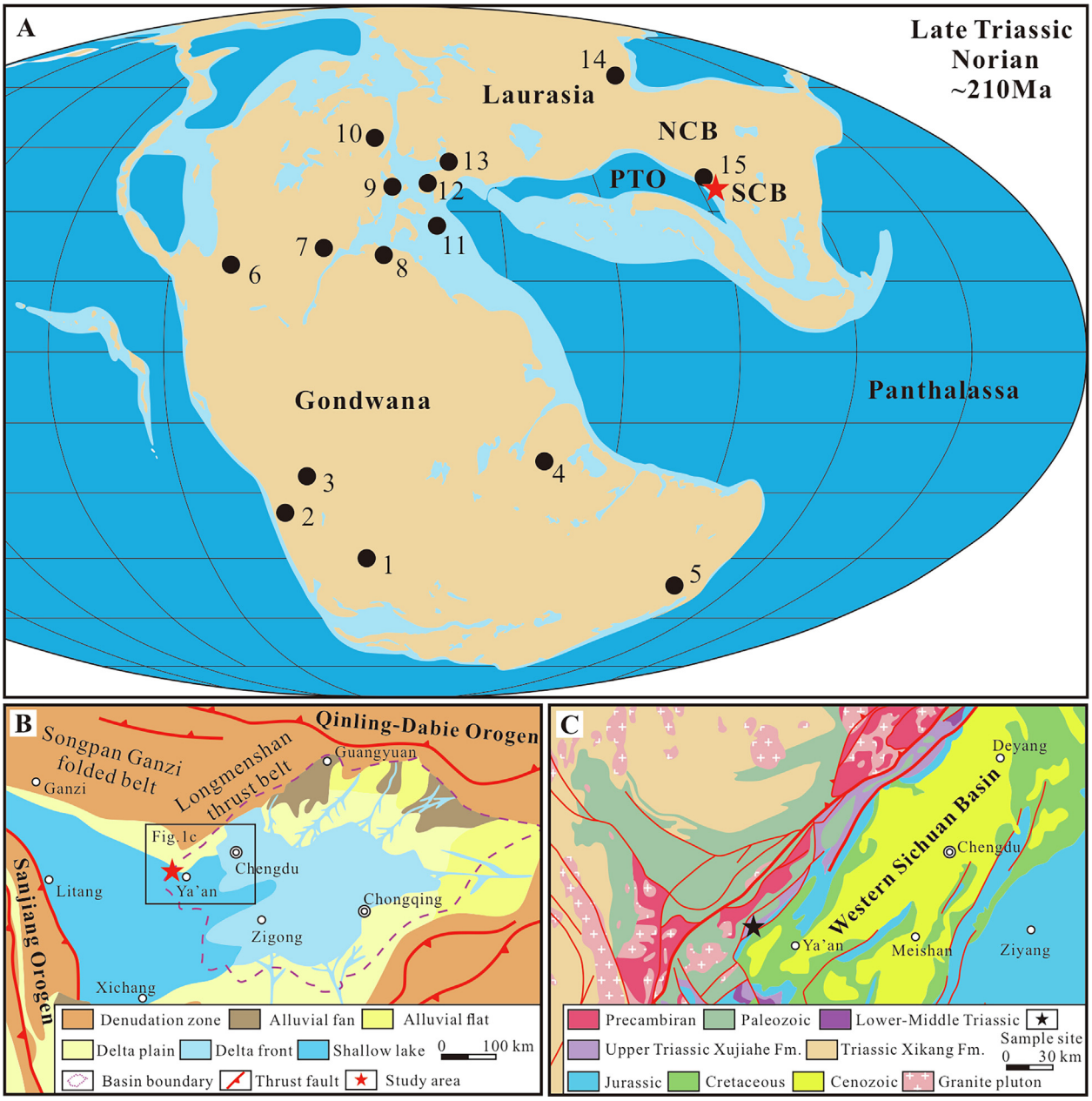

Fig. 1. (A). Distribution of main theropod-bearing deposits and track sites in the Late Triassic (1. Karoo basin, South Africa; 2. Bermejo Basin, Argentina; 3. Paraná Basin, Brazil; 4. Pranhita-Godavari Basin, India; 5. Sydney basin, Australia; 6. Chinle Formation and Dockum Group, western USA; 7. Newark Supergroup, eastern USA; 8. Argana Basin, Morocco; 9. Fissure-filling deposits, England; 10. Jameson Land, Greenland; 11. Southern Alps, Italy; 12. Germanic Basin, Germany; 13. Poręba site, Poland; 14. Junggar Basin, northwestern China; 15. Sichuan Basin, South China; NCB = North China Block; SCB = South China Block; PTO = Paleo-Tethys Ocean; red star represents the location of study area; modified after Langer et al., 2010; Klein and Lucas, 2010; Scotese, 2014; Whiteside et al., 2015; Olsen et al., 2022), (B). Simplified tectonic paleogeographic map of Sichuan Basin in the Late Triassic (modified after Zhu et al., 2017), and (C). Regional geological map of the western Sichuan Basin (modified after Mu et al., 2019). (For interpretation of the references to colour in this figure legend, the reader is referred to the web version of this article.)

the territory. However, this cannot explain the apparent absence, or rarity, of dinosaurs there, because the SCB joined the North China Block (NCB) in the Late Permian–Early Triassic during subduction and closure of the Mianlue Ocean (Wu and Zheng, 2013; Dong and Santosh, 2016). At this point, the SCB extended southward as a "peninsula" in eastern Tethys (Scotese, 2014), which made it possible for terrestrial plants and animals to enter overland.

Indeed, the South China region records basal archosaur tracks (*Chirotherium*) in the Middle Triassic (Anisian or Ladinian, Xing et al., 2013b), and dinosaur footprints (*Pengxianpus cifengensis*; *Eosauropus*) in the Late Triassic (Norian-Rhaetian, Yang and Yang, 1987; Lockley et al., 2013; Xing et al., 2013a, 2018), but only a few types of dinosaur footprints were reported, and the rocks were poorly dated.

Here, we report a large number of dinosaur footprints from the Late Triassic Xujiahe Formation, in the Tianquan area, Ya'an city, southwestern Sichuan Basin (Fig. 1B, C), which were first discovered and collected by Chengdu University of Technology (CDUT) in 1989. As one of the oldest records of dinosaurian tracks from China, we provide detrital zircon U-Pb ages that constrain the maximum depositional age of the footprint-bearing sediments. These

add to our knowledge of the oldest dinosaurs from eastern Tethys, important for understanding the diversification and migration of early dinosaurs in the Late Triassic.

2. Geological setting

As a compound continent, the SCB consists of the Yangtze Block in the northwest and the Cathaysia Block in the southeast, parts of the eastern Tethyan region. The SCB separated from the NCB along the Qinling-Dabie-Sulu Orogenic Belt in the early Mesozoic (Dong and Santosh, 2016; Mu et al., 2019; Liu et al., 2021). Located in the northwestern margin of the SCB, the Sichuan Basin is a large NE-SW-striking tectonic sedimentary basin, which was bounded by the Longmen Shan Thrust Belt to the west and the Qinling Orogenic Belt to the north. This basin experienced Late Sinian (Neoproterozoic)-to-Middle Triassic marine carbonate platform deposition, Late Triassic-to-Late Cretaceous terrestrial basin deposition, and subsequent exhumation and modification (Zhu et al., 2017; Deng et al., 2019; Liu et al., 2021). During the Late Triassic, the Sichuan Basin was uplifted and reoriented as a southwestward dipping foreland basin that received abundant detrital sediments from the surrounding highlands in response to the Indosinian Orogeny (Fig. 1B; Luo et al., 2014; Zhu et al., 2017; Mu et al., 2019; Chen et al., 2021). Stratigraphically, the Upper Triassic sequences are divided from bottom to top into the (marine) Ma'antang and Xiaotangzi formations and (non-marine) Xujiahe Formation, separated unconformably from the underlying Middle Triassic Leikoupo Formation and the overlying Lower Jurassic Baitianba Formation in the western Sichuan Basin (Fig. 2a, Xu et al., 2010; Mu et al., 2019).

The Xujiahe Formation comprises mainly gray or dark gray mudstones, shales, and grayish-yellow siltstones and sandstones, deposited in fluvial-delta-lacustrine environments within a terrigenous system (Chen et al., 2006; Li et al., 2017; Zhu et al., 2017; Wang et al., 2021). Generally, the Xujiahe Formation consists of five members (T_3x^2 to T_3x^6) in the western Sichuan Basin, among which the T_3x^3 and T_3x^5 members are dominated by gray mudstones and black shales interbedded with thin coal seams and light gray or grayish-yellow siltstones and sandstones, while the T_3x^2, T_3x^4 and T_3x^6 members are characterized by thick-bedded medium- to coarse-grained sandstones, with thin layers of siltstones, gray mudstones and thin coal beds (Fig. 2a; Deng et al., 2019; Yang et al., 2019).

The Xujiahe Formation in the western Sichuan Basin is well known for abundant fossil plants, invertebrate fossils, and occasional dinosaur tracks (Chen et al., 2006). The dinosaurian footprint *Pengxianpus cifengensis* was described and named by Yang and Yang (1987) and re-discussed by Lockley et al. (2013) and Xing et al. (2013a). In addition, some theropod, sauropodomorph, and archosaur tracks were reported in recent years from the Xujiahe Formation and the contemporaneous Baoding Formation in the SCB (Wang et al., 2005; Xing et al., 2014a, b, 2018). The geological

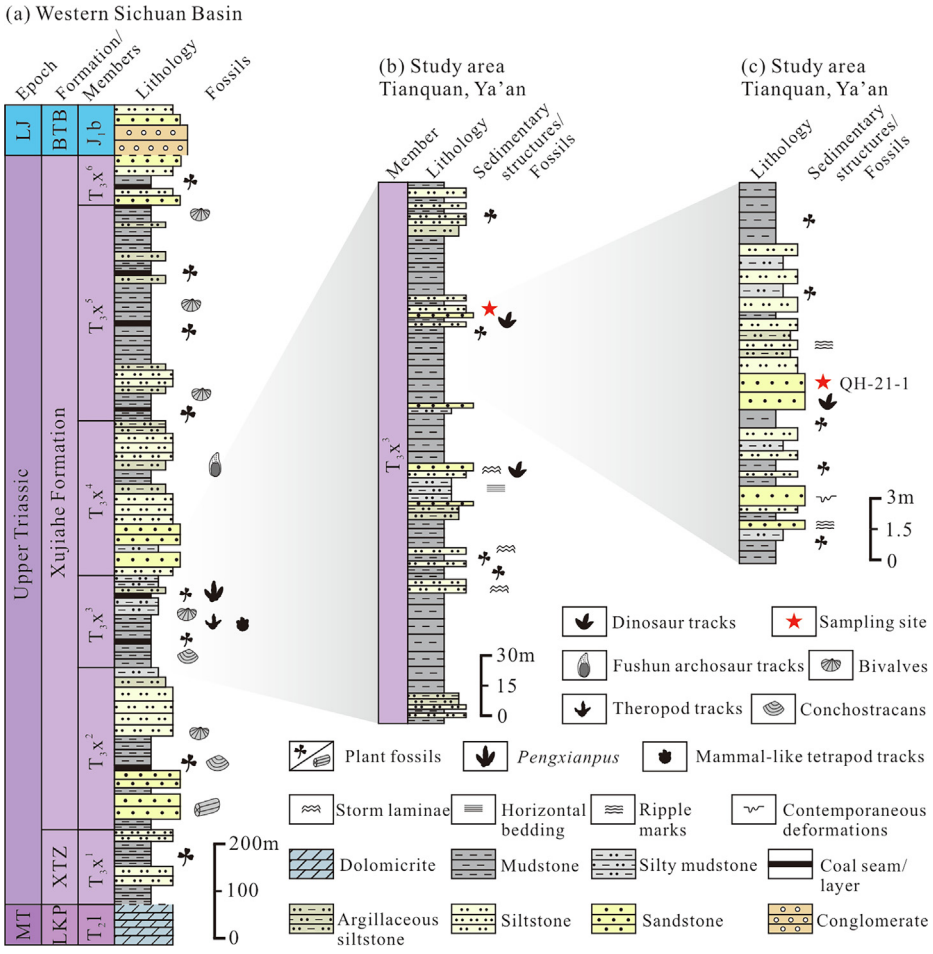

Fig. 2. (a) Stratigraphic column of the Upper Triassic Xujiahe Formation in the western Sichuan Basin, South China, showing abundance of fossil plants, bivalves, conchostracans, and dinosaur footprint fossils (Wang et al., 2005; Xing et al., 2013a, 2014a; Tian et al., 2016; Yang et al., 2019; Xu et al., 2021); (b) and (c). Measured lithology columns of the T_3x^3 in study area, showing the distribution of dinosaur footprints and sampling site for detrital zircon U-Pb dating. Abbreviations: MT, Middle Triassic; LJ, Lower Jurassic; LKP, Leikoupo Formation; XTZ, Xiaotangzi Formation; BTB, Baitianba Formation.

age of the Xujiahe Formation has been constrained to Norian-Rhaetian based on fossil bivalves (*Yunnanophorus boulei-Trigonodus keuperinus* assemblage zone), ostracods (*Sulcocythere-Oncocythere-Darwinulla* assemblage), plants (*Dictyophyllum nathorsti-Clathropteris meniscioides* flora), and sporomorphs (Chen et al., 2006; Li et al., 2017). Radioisotopic age data from detrital zircon U-Pb geochronology reveal the maximum depositional age of the Xujiahe Formation should be 228 ~ 203 Ma (Luo et al., 2014; Zhang et al., 2015; Mu et al., 2019). Further, Ran et al. (2016) reported a U-Pb age of 214.7 ± 1.6 Ma from a pyroclastic layer in T_3x^5, which was relatively older than the age based on astronomically tuned magnetostratigraphy of the Xujiahe Formation in the Sichuan Basin (207.2 ~ 201.3 Ma, Li et al., 2017).

The dinosaur tracks reported here were first discovered during a regional geological survey in 1989 on the north bank of the Tianquan river, under the Qingjiang Bridge, in Wuan Village, Tianquan Country, Ya'an City, Sichuan Province, China (GPS: 30.090° N, 102.727° E). It is worth noting that Wang et al. (2005) also reported two theropod footprints from the same section close to this track site (Xing et al., 2013a). In this section, abundant fossil plants and trace fossils occur in thick-bedded gray or dark-gray siltstones and mudstones, and ripple marks and synsedimentary deformation structures are common in gray-yellow sandstone interlayers, which indicate a shallow lake or swamp dominated environment (Fig. 2b, c and Fig. 3).

3. Materials and methods

3.1. Dinosaur tracks

A total of 16 sandstone slabs (numbered from S1 to S16) with dinosaur footprints were collected from the T_3x^3, in the Tianquan area, now placed in the dinosaur warehouse of the Museum of Chengdu University of Technology. Five of these 16 slabs (S1–S5) displayed 22 well-preserved dinosaur footprints, forming six trackways with two to four successive imprints each, and four isolated tracks. All these footprints left on silty mudstones were preserved as convex hyporeliefs on the lower surfaces of gray-yellow fine-grained sandstones. These slabs were photographed with a Canon EOS 6D mark Ⅱ with a flash storb supported, then outlined and digitalized in CorelDRAW (2020) based on the photos to show details.

We took various measurements from the fossil tracks and trackways. Footprint length (FL), width (FW), digit length (DL), digit divarication angles, pace length (PL), stride length (SL), pace angulation (PA), and trackway width (TW) were measured following the methods proposed by Li (2015). In addition, we assessed the projection ratio (Olsen et al., 1998), which is a measure of how far digit III projects beyond the tips of digits II and IV. Because this projection can vary largely due to the different digit divarication angle II-IV (θ), Olsen et al. (1998, p. 586) proposed a correction to the length of the rear of the phalangeal part of the pes (R) by trigonometrically adjusting R as if digits II and IV were parallel to digit III. This trigonometric approximation for this 'corrected' R, R' is:

$$R\prime = R * [1/\cos(\theta/2)].$$

The 'corrected' projection ratio (P) therefore is:

$$P = R\prime / (T - R\prime),$$

where T is the length of the phalangeal part of the pes skeleton (in other words, the digit length) and $T - R'$ is the 'corrected' projection of digit III forward beyond II and IV. The data are listed in Supplementary Table 1.

3.2. Detrital zircon U-Pb dating

To constrain the age of the dinosaur footprints, we collected one sandstone sample from the dinosaur track site for detrital zircon U-Pb dating (sample: QH-21–1). Zircon grains were separated by standard heavy-liquid and magnetic methods, then elongated grains with better crystal shapes were hand-picked under the stereo microscope (Olympus SZX7). After that, these zircon grains were mounted in epoxy and polished to show internal structures for target selection, combined with cathodoluminescence (CL) images, transmitted, and reflected light micrographs, and further for laser ablation analyses. Detrital zircon LA-ICP-MS U-Pb dating was carried out at the State Key Laboratory of Oil and Gas Reservoir and Exploitation, Chengdu University of Technology, using an Agilent 7900 ICP-MS coupled with a 193 nm wavelength laser ablation system (Resolution LR) from Applied Spectra. Detailed instrumental parameters and operating conditions are those listed in Paton et al. (2010). Zircon quality monitor GJ-1 and Plesovice were analyzed as unknown samples together with 91,500 standards and our zircon samples. Off-line data processing, including section and integration of background and analyte signals, quantitative corrections of trace element data and zircon U-Pb ages, was conducted with the Excel-based *ICPMSDataCal 11.1* software (Liu et al., 2010). The detrital zircon U-Pb concordia diagram and weight mean age diagram were plotted with the *Isoplot 3.0* software (Ludwig, 2003). Details of zircon U-Pb ages are given in Supplementary Table 2.

4. Results

4.1. Dinosaur ichnology

4.1.1. Slab 1

There are two successive pes imprints in Slab 1 (S1), forming a trackway (T1, Fig. 4). The right pes imprint (T1-1) is unambiguous and better preserved compared to the left one (T1-2). The overall shape of the moderately sized tridactyl pes imprints with long and slender digits and elongate claw traces suggest typical characters of a bipedal theropod. Track T1-1 is nearly symmetrical along the digit III axis, with a footprint length of 12.3 cm, and the length/width ratio is 1.1, digit III is the longest digit with a length of 7.5 cm, and the digit III projection ratio is 1.2. The divarication between the digits is relatively wide, with angles of II 40.8° III 38.1° IV in track T1-1. The pace length between T1-1 and T1-2 is 44.4 cm, and the estimated trackway width is 2.8 cm. Metatarsal phalangeal pad traces are visible, partially preserved in the proximal portion of digit IV (Fig. 4B, C), further measurements are provided in Supplementary Table 1.

4.1.2. Slab 2

There are nine pes imprints in Slab 2 (S2), including two trackways and an isolated footprint (Fig. 5). Trackway 2 (T2) consists of four successive tulip-shaped (U-shaped) tridactyl tracks, with digits connected with metatarsal phalangeal pad (Fig. 5A-E). Compared with track T2-4, tracks T2-1, T2-2, and T2-3 are indistinct and relatively deformed in morphology, possibly because of a wet and slippery substrate. Four footprints in trackway 2 are moderately sized, with an average length of 13.2 cm, and a mean length/width ratio of 1.2. Digit III is the longest and forms the approximate symmetric axis of the imprint, digits II and IV are relatively shorter. The average divarication angle between digits II and IV is 71.0°, and the angle between digits II and III is slightly larger than that between digits III and IV. The pace length between tracks ranges from 60.6 to 72.8 cm, and the stride length ranges

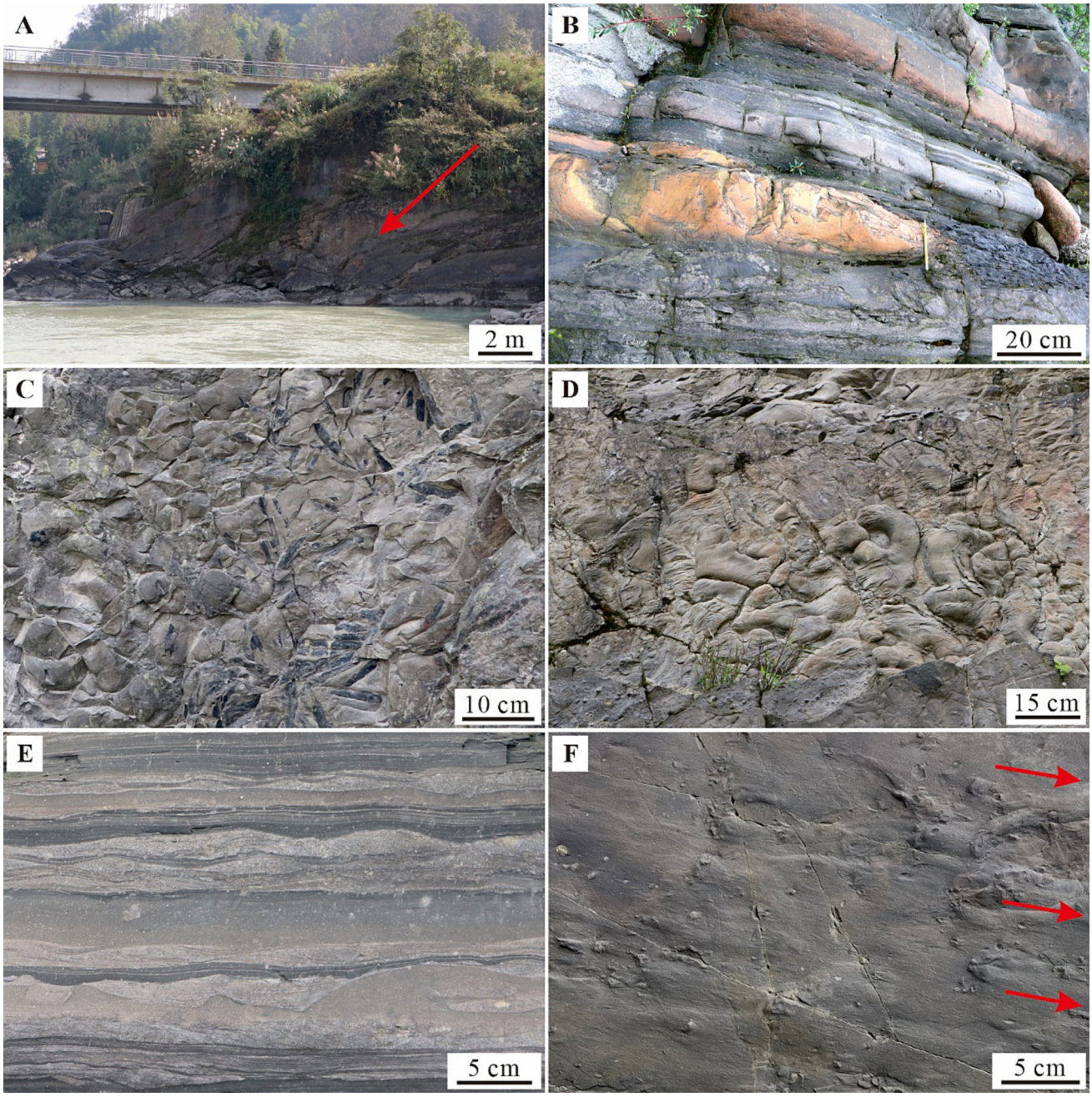

Fig. 3. Field photographs of the third member of the Xujiahe Formation (T_3x^3) at the dinosaur track locality. (A). Overview of the track site (red arrow indicates the site position of the tracks); (B) Gray and black argillaceous siltstone and mudstone interbedded with grayish yellow and apricot-colored sandstone (C). Plant fossils occurring in gray mudstone in the T_3x^3; (D). Soft-sediment deformation structures developed in the subface of gray-yellow siltstone; (E) Horizontal bedding and climbing ripple bedding from silty mudstone and siltstone; (F). Bottom scour casts showing the direction of water flow (red arrows) and a great number of vertical burrows seen in cross section. (For interpretation of the references to colour in this figure legend, the reader is referred to the web version of this article.)

from 126.6 to 133.2 cm. The pace angulation is up to 173.2°, with a narrow trackway width, from 0.4 to 14.5 cm.

Trackway 3 (T3) also consists of four successive pes imprints, with lily-shaped (V-shaped) outline and separated digit traces (Fig. 5A). Tracks T3-1 and T3-4 are better preserved, T3-2 is indistinct, while the digit III of T3-3 is broken (Fig. 5G-J). The average length of three complete tracks is 11.8 cm with a mean length/width ratio of 1.1. Digit III is the longest, followed by digits IV and II. The digit III projection ratio ranges from 1.0 to 1.4. Sharp claw traces are visible, in digit III being curved inward (Fig. 5K). The divarication angles between digits are II 37.9° III 29.8° IV on average. Pace length, stride length, and pace angulation between pes imprints show averages of 45.0 cm, 88.0 cm, and 166.8°, respectively. Trackway widths are relatively narrow, varying between 0.7 and 13.2 cm.

Footprint 1 (F1) is an isolated pes imprint preserved together with trackways 2 and 3, but showing an opposite walking direction compared with the other tracks (Fig. 5A). F1 is a small tetradactyl theropod imprint with digit I located postero-medially of digit II (Fig. 5F).

4.1.3. Slab 3

There are four pes imprints preserved on Slab 3 (S3), including two successive footprints that formed a trackway and two isolated

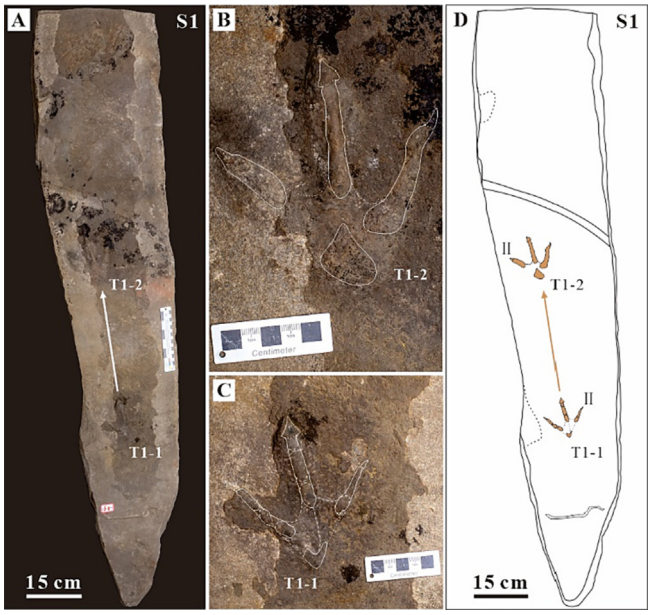

Fig. 4. Macrophotograph, close-up views and interpretative outline drawing of Slab 1. T1-1: the first imprint from partial trackway 1; II: showing the position of digit II.

tracks (Fig. 6A, G). The tracks from trackway 4 (T4) look like those of a typical tridactyl theropod, but the first track (T4-1) is incomplete and lacking digit II, while the other is indistinct (Fig. 6D, E). Track T4-2 is moderate-sized with a length of 12.9 cm and a length/width ratio of 1.2. Digit III is the longest (8.0 cm), followed by digit IV and II (6.3 cm and 5.7 cm, respectively). The divarication angle between digits II and IV is 67.1°, and the pace length between these two tracks is 44.8 cm.

Footprints 2 and 3 (F2 and F3) are two isolated imprints show similarities in morphology, which are probably tridactyl theropod tracks from overall shape, although they are poorly preserved (Fig. 6A, D, F). These two footprints are small with an average length of 10.8 cm. Digit traces are short and broad, and phalangeal pad traces are indistinct. For F3, the divarication angle between digit II and IV is II 17.7° III 17.3° IV, nearly symmetrical along the digit III axis.

4.1.4. Slab 4

Slab 4 (S4) preserves two successive pes imprints as positive hyporeliefs, forming trackway 5 (T5, Fig. 6H, I). The right foot imprint (T5-2) is better preserved than the left one, which shows the typical features of a tulip-shaped tridactyl theropod track with a length of 13.8 cm, and a length/width ratio of 1.3. The tracks are symmetrical approximately along the longest digit III axis, with

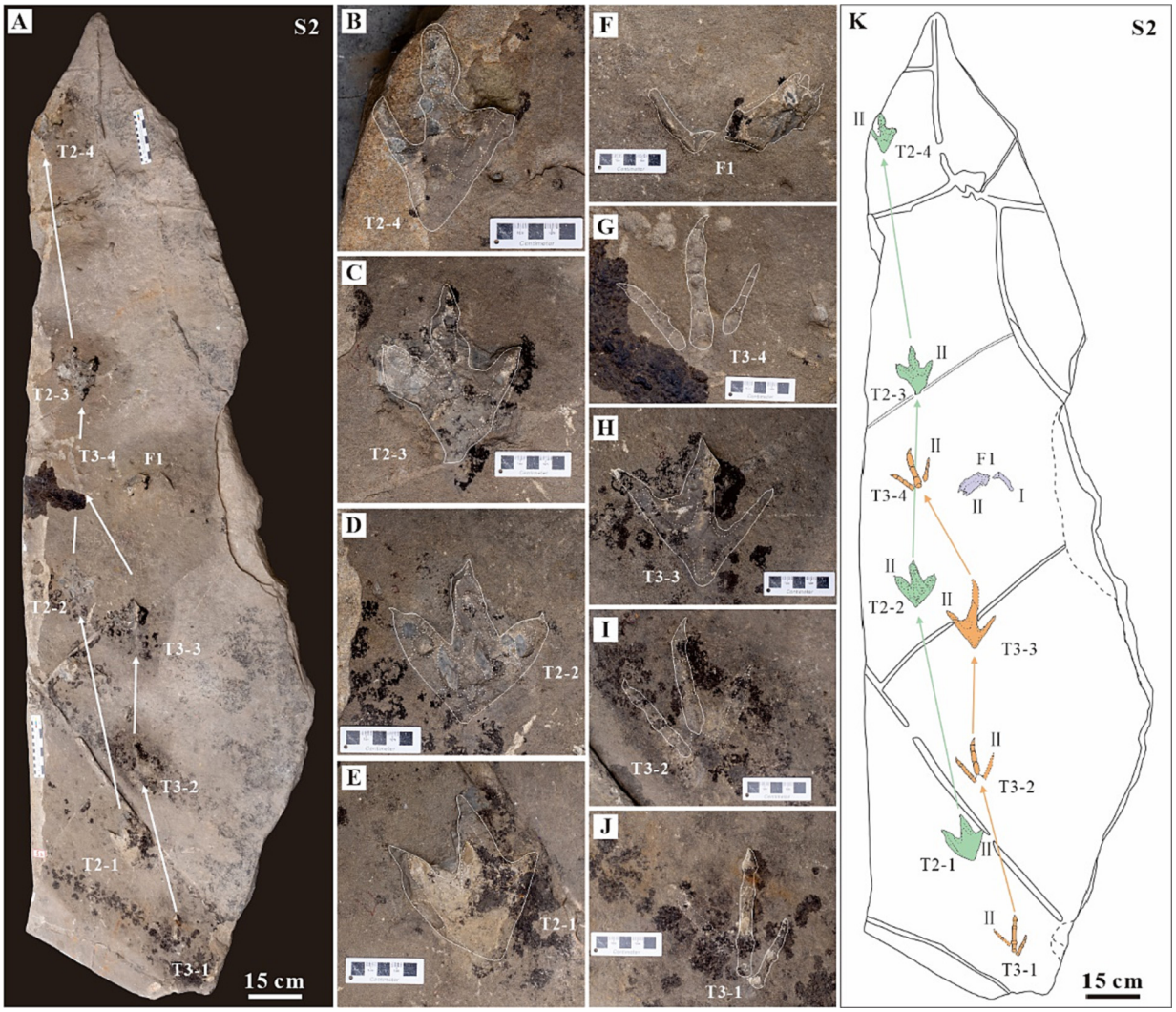

Fig. 5. Microphotograph, close-up views and interpretative outline drawing of Slab 2. T2-1: the first imprint from trackway 2; T3-1: the first imprint from the trackway 3; F1: isolated footprint 1; II: showing the position of digit II.

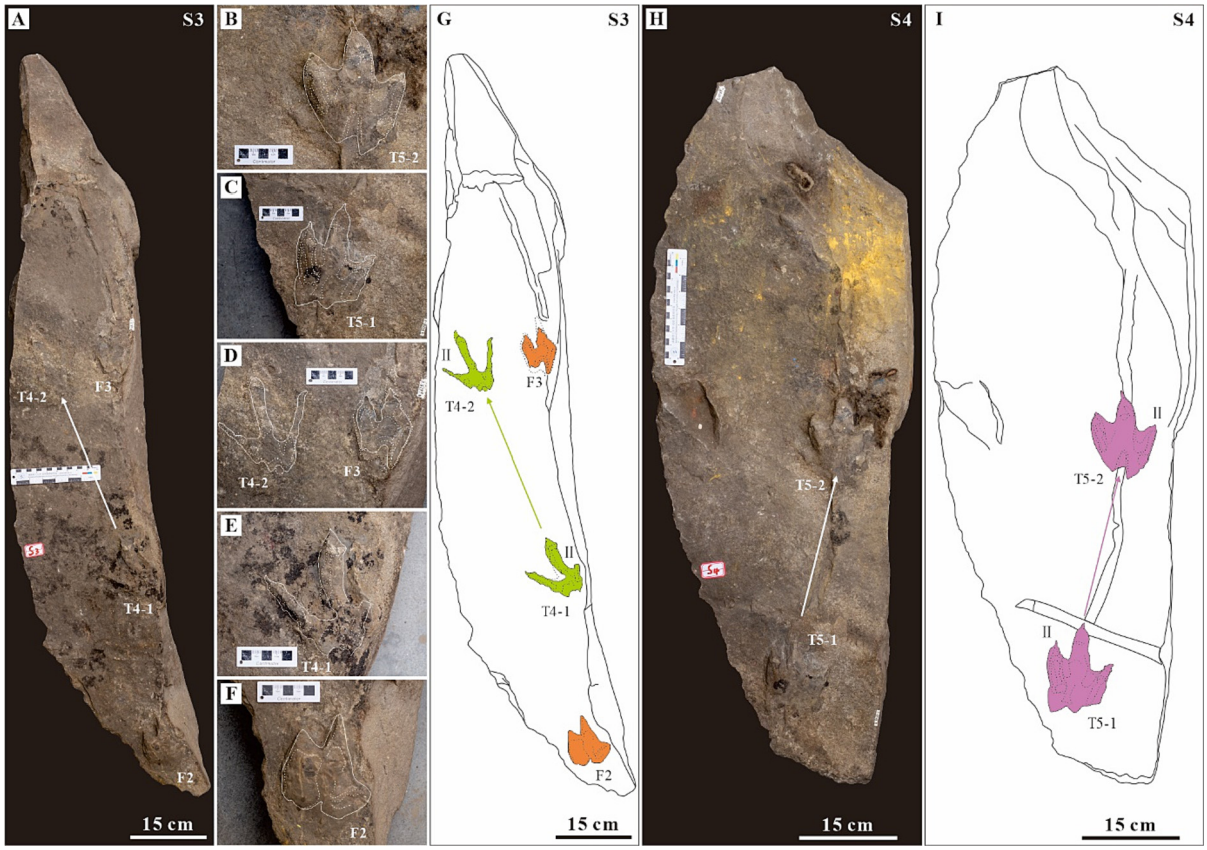

Fig. 6. Microphotographs, close-up views and interpretative outline drawings of Slab3 and Slab 4. T4-1: the first imprint from trackway 4; T5-1: the first imprint from trackway 5; F2: isolated footprint 2; F3: isolated footprint 3; II: showing the position of digit II.

partially visible sharp claw traces (Fig. 6B, C). The divarication angle between digits II and IV is 38.9° on average. The pace length between these two imprints is 35.5 cm.

4.1.5. Slab 5

There are five complete tracks on Slab 5 (S5), including four successive tridactyl theropod imprints that formed a trackway (T6) and an isolated footprint (F4) (Fig. 7A, F). For trackway 6, the first three are better preserved than the last one (T6-4) (Fig. 7B-E), these four pes imprints show relatively low mesaxony, indistinct digit pad traces, and wide digit hypex, with an average length of 12.2 cm, and a mean divarication angle between digits II and IV of 51.3°. The pace length, stride length and trackway width are 40.1 cm, 80.0 cm, and 3.0 cm on average, respectively, and the mean pace angulation is 172.7°.

Footprint 4 (F4) is an indistinct tridactyl theropod track with slender digits and claws, the footprint length is 17.1 cm, the length/width ratio is 1.6, digit III is the longest (16.3 cm), followed by digit IV and II (11.9 cm and 11.1 cm, respectively), and the divarication angle between digit II and IV is 38.8°.

4.2. Detrital zircon U-Pb ages

More than 200 euhedral zircon grains were picked under the stereo microscope. These angular and elongated grains show clear oscillatory zoning or homogeneous inner structure from CL images, with lengths between 50 and 200 μm. A total of 80 zircon grains were selected for U-Pb dating on the LA-ICP-MS, most of which have Th/U greater than 0.4 (95 %), and none of them less than 0.1, which indicates that these zircons were magmatic in origin with a short transport.

After calculation, 74 of the 80 grains yielded concordant ages with a discordance of $\leq$ 10 %, with 69 grains forming a major age population at ca. 298–216 Ma (Fig. 8A–C). In addition, four young zircon grains from the youngest age group gave a weight mean age of 218.4 ± 4.7 Ma (Fig. 8D), which represent the maximum sedimentary age of the strata. This indicates that the ages of the early dinosaurs from the Tianquan area should be no older than mid-Norian.

5. Discussion

5.1. Ichnotaxonomy and trackmaker identification

Key questions about the Xujiahe Formation dinosaur tracks are whether they all belong to a single ichnotaxon or represent different ichnotaxa, whether the ichnotaxon *Pengxianpus* established for such Chinese examples is valid, and what these tracks tell us about the groups of dinosaurs represented in the Late Triassic of the SCB and their behavior.

The ichnotaxon *Pengxianpus cifengensis* was established by Yang and Yang (1987) for two dinosaur footprints preserved as convex hyporeliefs from the Xujiahe Formation. These authors regarded *Pengxianpus* as a tetradactyl track made by a basal sauropodomorph dinosaur, but later study has shown that the supposed hallux is a fragment of mud crack sediment, and so the ichnotaxon is a tridactyl print more typical of theropod tracks (Wang et al., 2016). *Pengxianpus* is distinguished from *Eubrontes* by having more slender digits, less well-defined pad impressions, and a wider digit

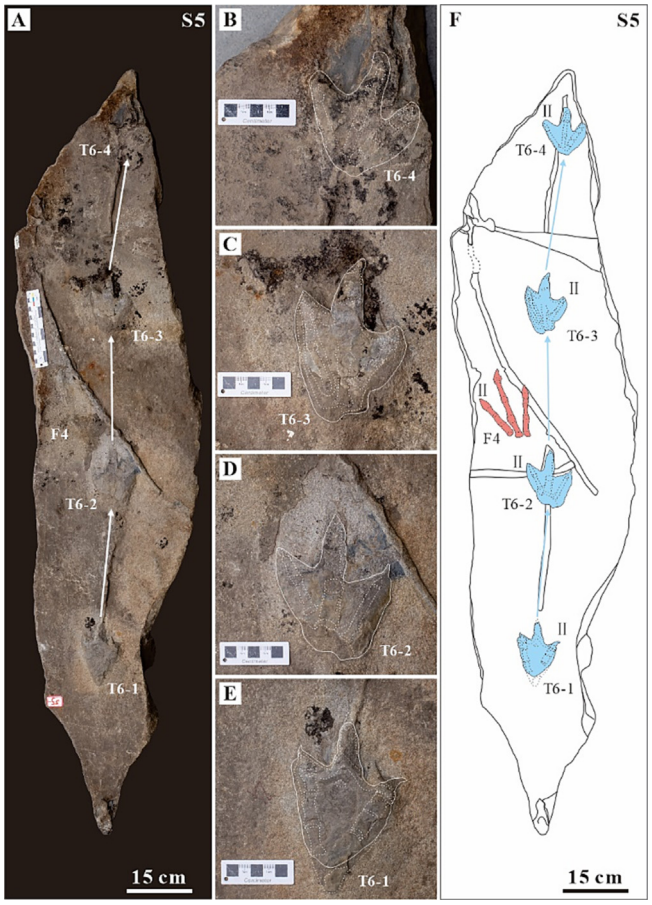

Fig. 7. Microphotograph, close-up views and interpretative outline drawing of Slab 5. T6-1: the first imprint from trackway 6; F4: isolated footprint 4; II: showing the position of digit II.

divarication, similar to the theropod ichnotaxon *Kayentapus* from the Late Triassic-Early Jurassic. Lockley et al. (2013), Xing et al. (2013a), and Wang et al. (2016) regard the ichnotaxon *Pengxianpus* as distinct from others, and therefore valid.

Such three-toed theropod footprints have long been recorded from the Late Triassic-Early Jurassic, particularly in North America (Lockley et al., 2011). Widely documented taxa include *Eubrontes* (Hitchcock, 1845), *Grallator* (Hitchcock, 1858), and *Anchisauripus* (Lull, 1904), as well as *Kayentapus* (Welles, 1971). These taxa should all be considered when identifying the tridactyl Xujiahe footprints.

Trackways 1 and 4 (T1 and T4) are consistent and show similarities with *Pengxianpus cifengensis* in morphology, including the nearly symmetrical mesaxonic digit configuration, slender digit traces, widely divaricated digits and metatarsal phalangeal pad traces on proximal digit IV (Fig. 9a, b). Trackway 3 (T3) has distinct characteristics of *Kayentapus*, including that the claw traces of digit III are oriented anteromedially, large digit divarication, and lily-shaped pes imprints (Fig. 9a, c). Trackways 2, 5 and 6 (T2, T5 and T6) also have similar shape, large digit divarication angles, and the moderate digit III projection ratio, showing some common features of *Pengxianpus* and *Kayentapus* (Fig. 9a, b, c). Isolated footprints 1–4 (F1 to F4) are indistinct small to moderately sized theropod tracks with relatively small digit divarication angles, which can be provisionally assigned to the *Grallator-Anchisauripus-Eubrontes* plexus (Fig. 9c, d).

The ichnotaxonomy of these Late Triassic and Early Jurassic tridactyl dinosaur tracks is complex, and discrimination between the ichnogenera can be tricky (Olsen et al., 1998; Lockley et al., 2013), so we applied a morphospace approach to make comparisons. We measured fifty tracks identified in the literature as *Eubrontes, Grallator, Anchisauripus*, *Kayentapus*, and *Pengxianpus*, and added our seventeen samples (T1–T6, F3 and F4), and plotted digit divarication angle (θ, II- IV) versus projection ratio. The data are listed in Supplementary Table 3. The morphospace plot shows differentiation of these type ichnogenera, with some overlap between *Grallator* and *Anchisauripus*, between *Anchisauripus, Eubrontes* and *Kayentapus,* and the type specimen of *Pengxianpus* falls in *Kayentapus* (Fig. 9e). Most of our specimens correspond to *Kayentapus-Pengxianpus*, while footprint 3 (F3) falls in the *Eubrontes* in morphospace as indicated (Fig. 9e). Therefore, the footprint morphospace analysis supports the result of the morphological comparison in ichnotaxonomy.

As for the makers of these tracks, they have all generally been assigned to theropods (e.g., Olsen et al., 1998; Lockley et al., 2013; Xing et al., 2013a, 2014a, 2018). Weems (2003) suggested that *Dilophosaurus* was the trackmaker of *Kayentapus hopii*, while the smaller track *Kayentapus minor* might have been made by the smaller theropod *Liliensternus* (Lockley et al., 2011). Therefore, the trackmaker of trackway 3 (T3) from Tianquan was probably a small-to-moderately-sized theropod like *Liliensternus*. Although we regard *Pengxianpus* as a valid ichnotaxon, if it is morphologically most similar to *Kayentapus* with slender digits and large digit divarication (Fig. 9), the trackmaker of *Pengxianpus* (T1 and T4) was presumably similar.

5.2. Ages of the earliest dinosaur tracks in China

The Late Triassic theropod tracks from the Sichuan Basin are the only direct evidence for the earliest dinosaurs in China, in the absence of skeletal fossils. However, only four dinosaur footprints (two trackways) were reported in the past several decades, including *Pengxianpus cifengensis* and two *Kayentapus*-like theropod footprints, from the Panlongqiao track site and the Tianquan site, from the third member of the Xujiahe Formation (Yang and Yang, 1987; Wang et al., 2005). Although these tracks were further analyzed later in terms of ichnotaxonomy, there were no accurate radioisotopic zircon age constraints (Lockley et al., 2013; Xing et al., 2013a). Our evidence connects diverse Late Triassic theropod tracks with a reliable dating as mid-Norian and a maximum depositional age of 218.4 ± 4.7 Ma (Fig. 8D).

To place our new data in context, we collected published detrital zircon and tuff zircon age data, and terrestrial biostratigraphic zonations of the Late Triassic in the Sichuan Basin, South China (Fig. 10). Detrital zircons from fine-grained muddy siltstones of the Ma'antang Formation yielded the youngest weighted mean age of 227.2 ± 1.1 Ma (n = 12) close to the Carnian/Norian boundary (Mietto et al., 2021). Two sandstone samples obtained from the Xiaotangzi Formation (T_3x^1) provided the youngest zircon age groups, with mean ages of 225.9 ± 3.6 Ma (n = 7), and 225.2 ± 3.0 Ma (n = 5), corresponding to early Norian (Chen et al., 2011). A tuff interlayer from the fourth member of the Xujiahe Formation (T_3x^4) yielded a consistent weighted mean U-Pb age of 214.7 ± 1.6 Ma (n = 28), which constrained the age of sedimentation (Ran et al., 2016). The youngest zircon grains obtained from the upper part of the Xujiahe Formation (T_3x^4–T_3x^6) gave a late Norian-Rhaetian age of 211–207 Ma (Zhang et al., 2015) (Fig. 10). All these zircon ages provide a reference calibration for the deposition time of the third member of the Xujiahe Formation (T_3x^3), from 225.2 to 214.7 Ma. However, bivalves and sporopollen fossils obtained from the middle to upper part of the Xujiahe Formation (with T_3x^3 included) give a relatively younger biostratigraphic constraint of late Norian–Rhaetian (Gou, 1998; Li et al., 2020). Considering that age interpretations based on biostratigraphic zones are often

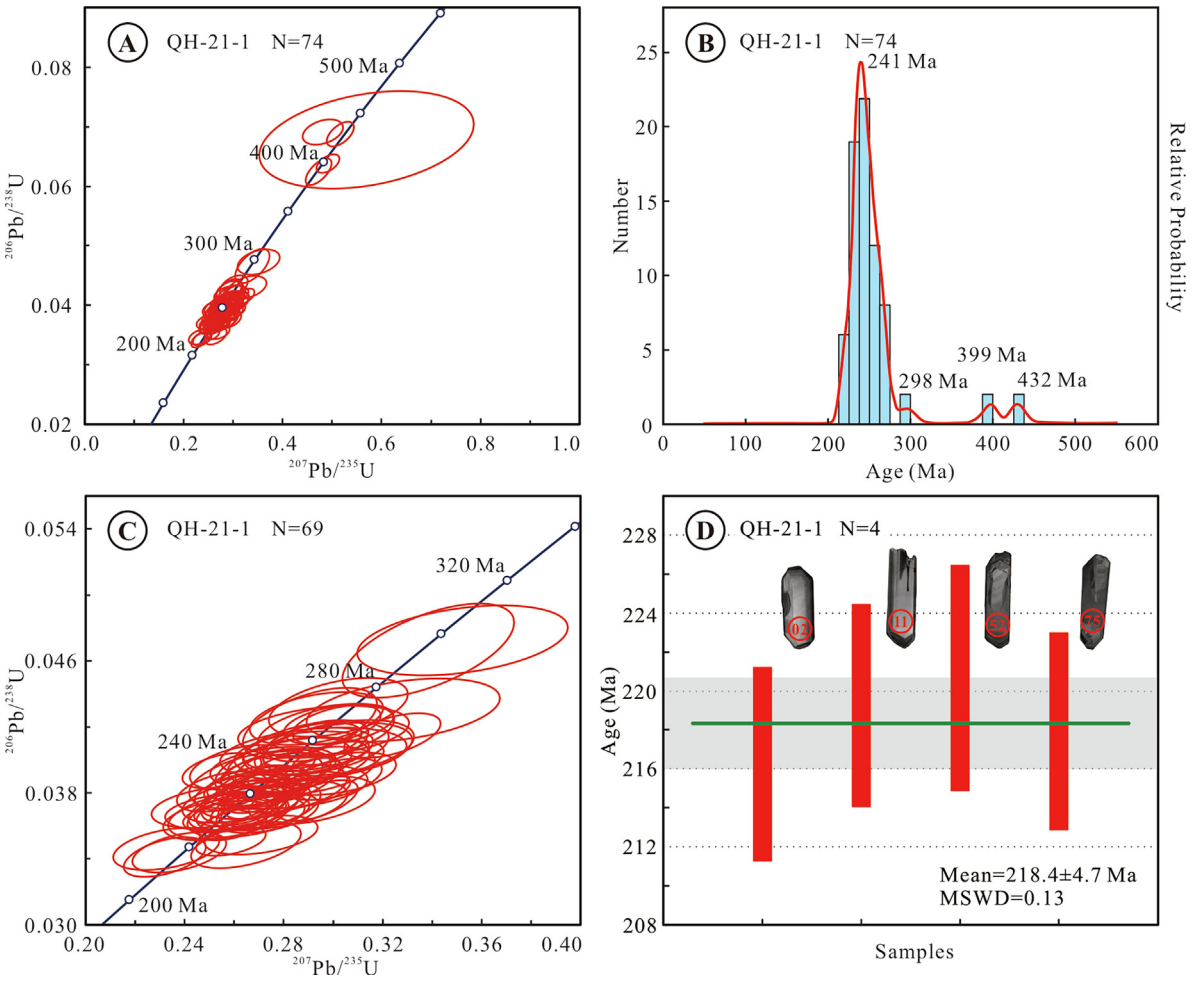

Fig. 8. U-Pb concordia plot for sandstone detrital zircons from sample QH-21–1 in Tianquan area (A); Probability density distribution curve of detrital zircon ages from sample QH-21–1 (B); U-Pb concordia plot for the younger group of zircon ages from sample QH-21–1 (C); Weighted mean age for the youngest age group of detrital zircons from sample QH-21–1 (D).

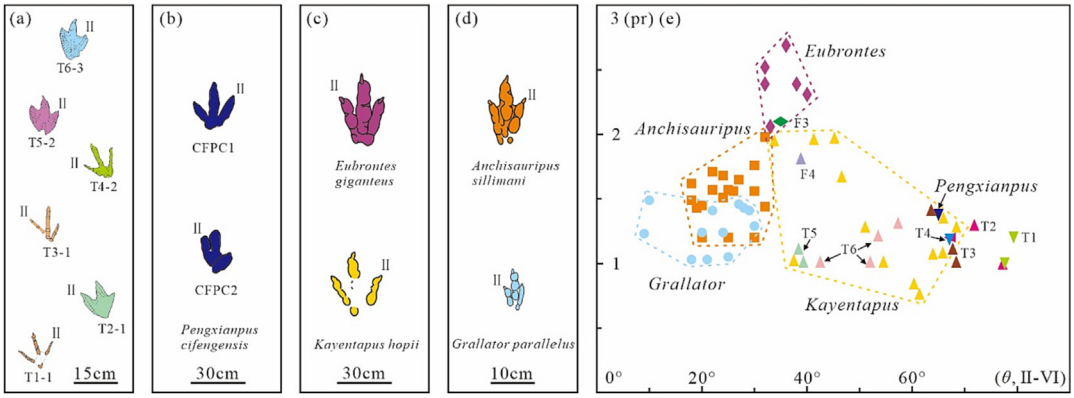

Fig. 9. Comparison of dinosaur tracks from the Tianquan area with *Pengxianpus*, *Kayentapus*, *Eubrontes*, *Grallator*, and *Anchisauripus* (a–d), and digit divarication angle (θ, II-IV) versus projection ratio morphospace plot of different kind of tracks (e) (data from Olsen et al., 1998; Lockley et al., 2011; Xing et al., 2013a; Li, 2015 and this study). Abbreviations: pr, projection ratio.

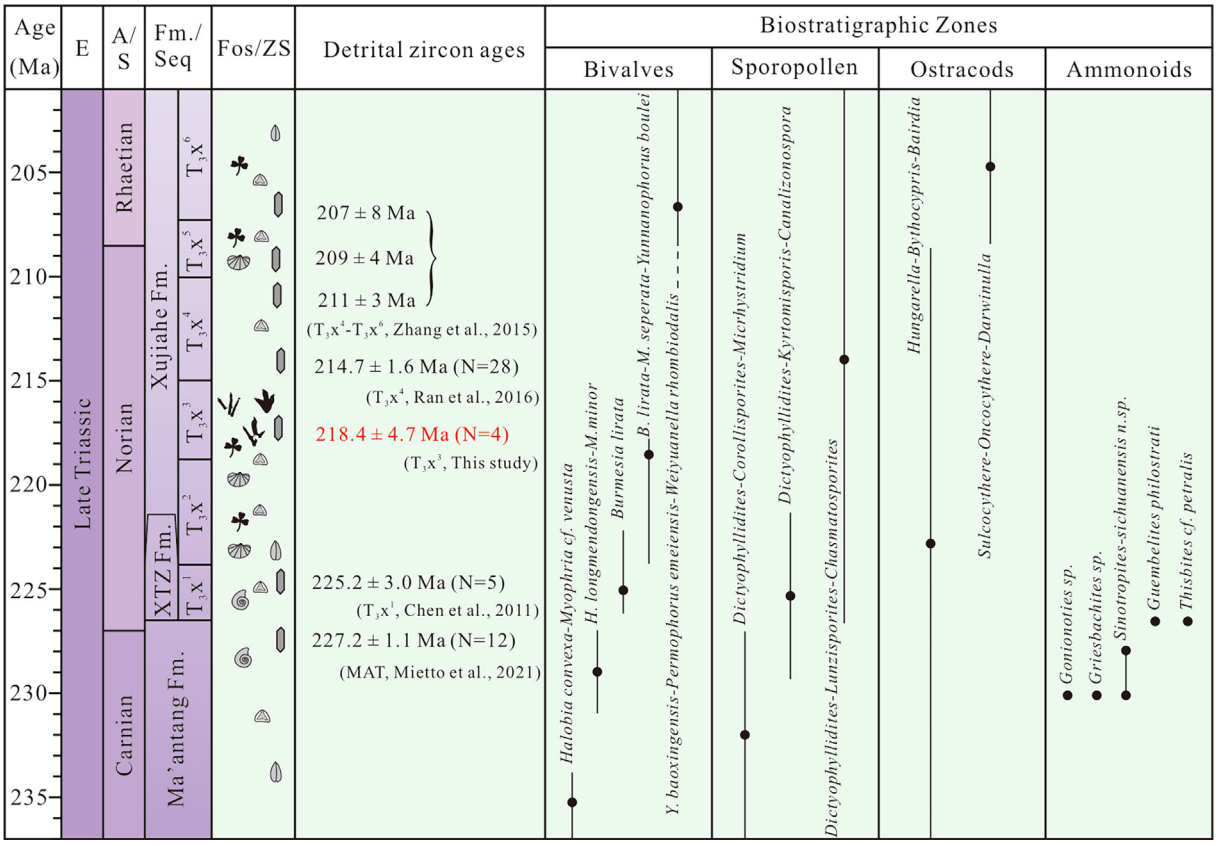

Fig. 10. Zircon U-Pb ages and biostratigraphic zonal range from the Late Triassic strata in the Sichuan basin, South China (zircon age data of different sequences are from Chen et al., 2011; Zhang et al., 2015; Ran et al., 2016; Mietto et al., 2021; and this study; Bivalve assemblage zones from Gou, 1998; Sporopollen assemblage zones from Li and Wang, 2016; Ostracod assemblage zones from Wang et al., 2010; Ammonoids from Mietto et al., 2021). Abbreviations: E, Epoch; A/S, Age/Stage; Fm./Seq, Formation/Sequence; Fos/ZS, Fossils/Zircon Samples (for explanation of fossil icons see Fig. 2); XTZ Fm., Xiaotangzi Formation; MAT, Ma'antang Formation.

inaccurate, we think it more likely that the concordant zircon ages with a weighted mean age of 218.4 ± 4.7 Ma (n = 4) in this study correspond well with the age of sedimentation (in T_3x^3), marking the age of the earliest dinosaur tracks in China.

5.3. Norian environments, migration and evolution of early dinosaurs in the eastern Tethys

The most significant feature of the Norian environment was a 'U-shaped' climate change (warming cycle) from early warm conditions to long-term cooling, and then back to a distinct warming event during the middle-late Norian. Paleotemperature evidence comes from $\delta^{18}O$ from conodont apatite and conodont oxygen isotope thermometry, and atmospheric pCO_2 estimated from pedogenic carbonates (Fig. 11A, B; Trotter et al., 2015; Schaller et al., 2015; Sun et al., 2020). This is supported by the observation of paleoclimate fluctuation based on plant and wood fossils (Tian et al., 2016; Xu et al., 2021), palynological assemblages (Lu et al., 2019; Li et al., 2020), and trace element fingerprints (Yang et al., 2019) from the Xujiahe Formation in the Sichuan Basin, that also reveal a persistent Norian warming trend (T_3x^3) after a relatively cool stage (T_3x^2) (Fig. 11C). Analogous to the argument that the mid-Carnian warming event recorded by a negative excursion of $\delta^{18}O_{phos}$ coincides with the global CPE that witnessed the turnover of marine and terrestrial ecosystems and the diversification of dinosaur clades (Trotter et al., 2015; Shi et al., 2017; Bernardi et al., 2018; Jin et al., 2022), we suggest that the mid-late Norian warming event and humid pulse corresponded to a warmer climate transition after the T_3x^3 in South China that was of great significance for paleoecological evolution, such as the emergence of early dinosaurs in the eastern Tethys.

The dinosaur footprints we report here, together with other tracks from the Xujiahe Formation in South China, namely indeterminate theropod footprints (Wang et al., 2005; Xing et al., 2013a), *Pengxianpus cifengensis* from the Panlongqiao track site (Yang and Yang, 1987; Xing et al., 2013a), and sauropodomorph tracks from the Yiguoyao track site (cf. *Eosauropus*, Xing et al., 2018), are the earliest dinosaur track records in the eastern Tethys. It is worth noting that most of the footprints are medium-to-small-sized tridactyl theropod tracks from the third member of the Xujiahe Formation, but with the addition of several larger sauropodomorph dinosaur tracks from the upper part of this formation. The mid-Norian relatively wetter and warmer shore-lake paleoenvironment in the western Sichuan Basin presumably enabled these small carnivorous or omnivorous theropods to thrive, as well as the later large-bodied herbivorous sauropodomorph dinosaurs. The first appearance of early dinosaurs in eastern Tethys, in a context of rapidly and dramatically fluctuating Norian environments, matches similar changes in temperature, precipitation, and atmospheric pCO_2 elsewhere (Whiteside et al., 2015; Lu et al., 2019; Olsen et al., 2022). The extremely high CO_2 concentration in the Norian led to a 'hothouse' earth with tropical lower paleolatitudes and temperate mid-high paleolatitudes.

Paleoclimatic conditions and the thermal physiology of tetrapod groups determined their distribution patterns. Ectothermic pseudosuchian archosaurs (crocodylians and their relatives) occupied a narrow and restricted range of tropical paleoclimates with highest species richness at the paleoequator, while endothermic,

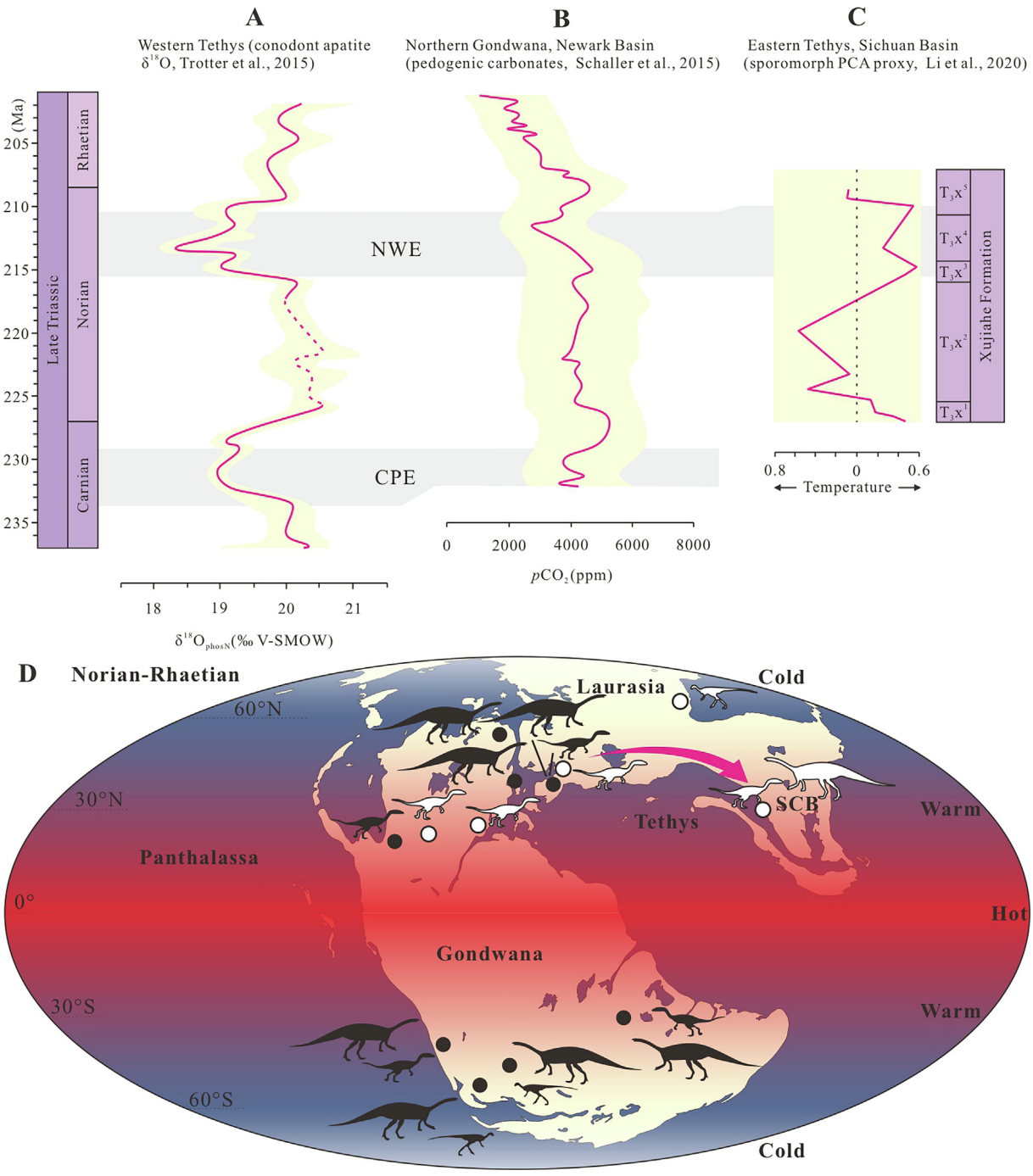

Fig. 11. Late Triassic paleoclimate changes as indicated by conodont apatite $\delta^{18}O$ (A, Trotter et al., 2015), atmospheric pCO_2 estimated from pedogenic carbonates (B, Schaller et al., 2015), sporomorph principal components analysis (PCA) proxy (C, Li et al., 2020), and Norian-Rhaetian paleolatitudinal and paleoclimate zones showing the potential direction of migration of dinosaur fauna on the Tethys rim (D, modified after Scotese, Langer et al., 2010; Lockley et al., 2011; Scotese, 2014; Whiteside et al., 2015; Olsen et al., 2022). Black and white silhouettes of dinosaurs represent sites of their remains and tracks, respectively. Abbreviations: NWE, Norian Warming Event; CPE, Carnian Pluvial Episode.

mesothermic or insulated (bearing protofeathers) avemetatarsalians (early dinosaurs and pterosaurs) exhibited relatively wider paleoclimatic ranges and paleolatitudinal distributions with higher richness at mid-paleolatitudes or even in polar regions (Dunne et al., 2021; Olsen et al., 2022). Considering that the revised Norian paleolatitude of the South China Block is about 29°N (Li et al., 2017), the paleolatitudinal biochores determined that the origin of early dinosaurs, with small theropods mainly in South China, eastern Tethys in the Late Triassic (mid-Norian) could be from the western Tethys regions that were located at similar mid-paleolatitudes in the northern hemisphere (Fig. 11D). As *Kayentapus* and its possible trackmaker *Liliensternus* were discovered in the Late Triassic of the western Tethys (such as Poland and France, Niedźwiedzki, 2005; Ezcurra and Cuny, 2007; Lockley et al., 2011), further support that the early dinosaurs with *Kayentapus*-dominated tracks in South China (eastern Tethys) presumably migrated in from the western Tethys.

The abundance of small to moderately sized tridactyl pes imprints from the Tianquan area lets us catch a glimpse of a stable theropod population that lived in South China. Further, these

theropod tracks from eastern Tethys match the timing of the early rise and rapid radiation of dinosaurs during the Late Triassic (mid-Norian) associated with fluctuating paleoclimatic extremes.

6. Conclusion

Abundant dinosaur track specimens from the Upper Triassic Xujiahe Formation (T_3x^3) of the Tianquan track site, Sichuan Basin, South China, represent one of the earliest records of dinosaurs from the Late Triassic of the eastern Tethys realm. All these dinosaur footprints are small, functionally tridactyl theropod tracks. Most of the tracks display large divarication angles between digits and are provisionally assigned to cf. *Pengxianpus* isp. and cf. *Kayentapus* isp., others are similar to well-known tracks of the *Grallator-Anchisauripus-Eubrontes* plexus. Detrital zircon U-Pb radioisotopic dating gives a weighted mean age of 218.4 ± 4.7 Ma, representing the maximum deposition age of the dinosaur track-bearing sequences. Latitudinal sorting according to thermal physiology determined that the mid-Norian dinosaurs in South China could have migrated from western Tethys regions at similar paleolatitudes, especially under the dramatically fluctuating paleoclimates of the Norian. These theropod tracks from South China, eastern Tethys help to illustrate the rise of dinosaurs to ecological dominance during the mid-Norian.

CRediT authorship contribution statement

Shenyuan Peng: Investigation, Data curation, Formal analysis, Writing – original draft. **Jian Liu:** Resources, Supervision. **Michael J. Benton:** Investigation, Methodology, Writing – review & editing. **Xin Jin:** Conceptualization, Supervision, Writing – review & editing. **Zhiqiang Shi:** Conceptualization, Investigation, Writing – review & editing, Funding acquisition.

Declaration of Competing Interest

The authors declare that they have no known competing financial interests or personal relationships that could have appeared to influence the work reported in this paper.

Acknowledgements

We thank Xiaomei Zhou and Dan Qiao from Chengdu University of Technology and Nereo Preto and Qiangwang Wu from Padova University (Italy) for their assistance in the field work. This study is founded by Department of Science and Technology of Sichuan Province, China (Grant No. 2021YJ0353) and Natural Science Foundation (Grant No. 41572085) of the Chinese Ministry of Science and Technology. We also appreciate constructive suggestions from the editor and reviewers.

Appendix A. Supplementary data

Supplementary data to this article can be found online at https://doi.org/10.1016/j.gr.2023.02.003.

References

Benton, M.J., Bernardi, M., Kinsella, C., 2018. The Carnian Pluvial Episode and the origin of dinosaurs. J. Geol. Soc. London 175, 1019–1026.
Bernardi, M., Gianolla, P., Petti, F.M., Mietto, P., Benton, M.J., 2018. Dinosaur diversification linked with the Carnian Pluvial Episode. Nat. Commun. 9, 1499.
Brusatte, S.L., Niedźwiedzki, G., Butler, R.J., 2011. Footprints pull origin and diversification of dinosaur stem lineage deep into Early Triassic. Proc. R. Soc. B 278, 1107–1113.
Chen, P.J., Li, J.J., Matsukawa, M., Zhang, H.C., Wang, Q.F., Lockley, M.G., 2006. Geological ages of dinosaur-track-bearing formations in China. Cretac. Res. 27, 22–32.
Chen, Y., Liu, S.G., Li, Z.W., Deng, B., Zeng, X.L., Lin, J., 2011. LA-ICP-MS detrital zircon U-Pb geochronology approaches to the sediment provenance of the western Sichuan foreland basin and limited uplift of the Longmen Mountains during the early stage of Late Triassic. Geotecton. Metallog. 35, 315-323 (in Chinese with English abstract).
Chen, H.D., Liu, L., Lin, L.B., Wang, X.L., Wang, Z.W., Yu, Y., Zeng, J., Li, P.W., 2021. Depositional responses of Xujiahe Formation to the uplifting of Longmenshan during the Late Triassic, Western Sichuan Depression. Oil Gas Geol. 42, 801-815 (in Chinese with English abstract).
Da Rosa, A.A.S., 2015. Geological context of the dinosauriform-bearing outcrops from the Triassic of Southern Brazil. J. S. Am. Earth Sci. 61, 108–119.
Dal Corso, J., Bernardi, M., Sun, Y.D., Song, H.J., Seyfullah, L.J., Preto, N., Gianolla, P., Ruffell, A., Kustatscher, E., Roghi, G., Merico, A., Hohn, S., Schmidt, A.R., Marzoli, A., Newton, R.J., Wignall, P.B., Benton, M.J., 2020. Extinction and dawn of the modern world in the Carnian (Late Triassic). Sci. Adv. 6. eaba0099.
Deng, T., Li, Y., Wang, Z.J., Yu, Q., Dong, S.L., Yan, L., Hu, W.C., Chen, B., 2019. Geochemical characteristics and organic matter enrichment mechanism of black shale in the Upper Triassic Xujiahe Formation in the Sichuan basin: Implications for paleoweathering, provenance and tectonic setting. Mar. Pet. Geol. 109, 698–716.
Dong, Y.P., Santosh, M., 2016. Tectonic architecture and multiple orogeny of the Qinling Orogenic Belt, Central China. Gondw. Res. 29, 1–40.
Dunne, E.M., Farnsworth, A., Greene, S.E., Lunt, D.J., Butler, R.J., 2021. Climatic drivers of latitudinal variation in Late Triassic tetrapod diversity. Palaeontology 64, 101–117.
Ezcurra, M.D., Cuny, G., 2007. The coelophysoid *Lophostropheus airelensis*, gen. nov.: a review of the systematics of "*Lilienstern*us" *airelensis* from the Triassic-Jurassic outcrops of Normandy (France). J. Vertebr. Paleontol. 27, 73–86.
Ezcurra, M.D., Nesbitt, S.J., Bronzati, M., Dalla Vecchia, F.M., Agnolin, F.L., Benson, R. B.J., Egli, F.B., Cabreira, S.F., Evers, S.W., Gentil, A.R., Irmis, R.B., Martinelli, A.G., Novas, F.E., da Silva, L.R., Smith, N.D., Stocker, M.R., Turner, A.H., Langer, M.C., 2020. Enigmatic dinosaur precursors bridge the gap to the origin of Pterosauria. Nature 588, 445–449.
Gou, Z.H., 1998. The bivalve fauna from the Upper Triassic Xujiahe Formation in the Sichuan Basin. Sedimentary Facies Palaeogeography 18 (2), 22-31 (in Chinese with English abstract).
Hartung, J., Augustin, F.J., Kampouridis, P., Chure, D.J., 2021. A unique notostracan trace fossil assemblage from the Upper Triassic Chinle Formation (northeastern Utah, USA) and its paleoecological and paleoenvironmental implications. Palaeogeogr. Palaeoclimatol. Palaeoecol. 583, 110667.
Hitchcock, E., 1845. An attempt to discriminate and describe the animals that made the fossil footmarks of the United States, and especially of New England. Memoirs American Acad. Arts Sci. 3, 129–256.
Hitchcock, E., 1858. Ichnology of New England. In: Boston, W., 1974. A report on the sandstone of the Connecticut Valley, especially its fossil footmarks. Arno Press, New York.
Jin, X., Franceschi, M., Martini, R., Shi, Z.Q., Gianolla, P., Rigo, M., Wall, C.J., Schmitz, M.D., Lu, G., Du, Y.X., Huang, X.T., Preto, N., 2022. Eustatic sea-level fall and global fluctuations in carbonate production during the Carnian Pluvial Episode. Earth Planet. Sci. Lett. 594, 117698.
Klein, H., Lucas, S.G., 2010. Tetrapod footprints-their use in biostratigraphy and biochronology of the Triassic. Geol. Soc. Lond. Spec. Publ. 334, 419–446.
Lagnaoui, A., Klein, H., Voigt, S., Hminna, A., Saber, H., Schneider, J.W., Werneburg, R., 2012. Late Triassic tetrapod-dominated ichnoassemblages from the Argana Basin (Western High Atlas, Morocco). Ichnos 19, 238–253.
Lallensack, J.N., Klein, H., Milàn, J., Wings, O., Mateus, O., Clemmensen, L.B., 2017. Sauropodomorph dinosaur trackways from the Fleming Fjord Formation of East Greenland: Evidence for Late Triassic sauropods. Acta Palaeontol. Pol. 62, 833–843.
Langer, M.C., Ezcurra, M.D., Bittencourt, J.S., Novas, F.E., 2010. The origin and early evolution of dinosaurs. Biol. Rev. 85, 55–110.
Langer, M.C., Ramezani, J., Da Rosa, Á.A.S., 2018. U-Pb age constraints on dinosaur rise from south Brazil. Gondw. Res. 57, 133–140.
Li, L.Q., Wang, Y.D., 2016. Late Triassic palynofloras in the Sichuan Basin, South China: Synthesis and perspective. Palaeoworld 25, 212–238.
Li, L.Q., Wang, Y.D., Kürschner, W.M., Ruhl, M., Vajda, V., 2020. Palaeovegetation and palaeoclimate changes across the Triassic-Jurassic transition in the Sichuan Basin, China. Palaeogeogr. Palaeoclimatol. Palaeoecol. 556, 109891.
Li, M.S., Zhang, Y., Huang, C.J., Ogg, J., Hinnov, L., Wang, Y.D., Zou, Z.Y., Li, L.Q., 2017. Astronomical tuning and magnetostratigraphy of the Upper Triassic Xujiahe Formation of South China and Newark Supergroup of North America: Implications for the Late Triassic time scale. Earth Planet. Sci. Lett. 475, 207–223.
Li, J.J., 2015. Fascicle 8 (Serial no. 12) Footprints of Mesozoic reptilians and avians. In: Li, J.L. (ed.) Volume Amphibians, reptilians, and avians. Palaeovertebrata Sinica, Editorial Committee of Palaeovertebrata Sinica (in Chinese).
Liu, Y.S., Hu, Z.C., Zong, K.Q., Gao, C.G., Gao, S., Xu, J., Chen, H.H., 2010. Reappraisement and refinement of zircon U-Pb isotope and trace element analyses by LA-ICP-MS. Chin. Sci. Bull. 55, 1535–1546.
Liu, S.G., Yang, Y., Deng, B., Zhong, Y., Wen, L., Sun, W., Li, Z.W., Jansa, L., Li, J.X., Song, J.M., Zhang, X.H., Peng, H.L., 2021. Tectonic evolution of the Sichuan Basin, Southwest China. Earth-Sci. Rev. 213, 103470.

Lockley, M.G., Gierlinski, G., Lucas, S.G., 2011. *Kayentapus* revisited: notes on the type material and the importance of this theropod footprint ichnogenus. N. M. Mus. Nat. Hist. Sci. Bull. 53, 330–336.
Lockley, M.G., Li, J.J., Li, R.H., Matsukawa, M., Harris, J.D., Xing, L.D., 2013. A review of the tetrapod track record in China, with special reference to type ichnospecies: Implications for ichnotaxonomy and paleobiology. Acta Geol. Sinica (English Edition) 87, 1–20.
Lu, N., Wang, Y.D., Popa, M.E., Xie, X.P., Li, L.Q., Xi, S.N., Xin, C.L., Deng, C.T., 2019. Sedimentological and paleoecological aspects of the Norian-Rhaetian transition (Late Triassic) in the Xuanhan area of the Sichuan Basin, Southwest China. Palaeoworld 28, 334–345.
Lucas, S.G., 1998. Global Triassic tetrapod biostratigraphy and biochronology. Palaeogeogr. Palaeoclimatol. Palaeoecol. 143, 347–384.
Lucas, S.G., 2010. The Triassic timescale based on nonmarine tetrapod biostratigraphy and biochronology. Geol. Soc. Lond. Spec. Publ. 334, 447–500.
Ludwig, K.R., 2003. ISOPLOT 3.00: A Geochronological Toolkit for Microsoft Excel. Berkeley Geochronology Center, California, Berkeley, pp. 39.
Lull, R.S., 1904. Fossil footprints of the Jura-Trias of North America. Boston Soc. Natural History, Memoirs 5, 461–557.
Luo, L., Qi, J.F., Zhang, M.Z., Wang, K., Han, Y.Z., 2014. Detrital zircon U-Pb ages of Late Triassic-Late Jurassic deposits in the western and northern Sichuan Basin margin: constraints on the foreland basin provenance and tectonic implications. Int. J. Earth Sci. 103, 1553–1568.
Marsicano, C.A., Barredo, S.P., 2004. A Triassic tetrapod footprint assemblage from southern South America: palaeobiogeographical and evolutionary implications. Palaeogeogr. Palaeoclimatol. Palaeoecol. 203, 313–335.
Melchor, R.N., De Valais, S., 2006. A review of Triassic tetrapod track assemblages from Argentina. Palaeontology 49, 355–379.
Mietto, P., Jin, X., Manfrin, S., Lu, G., Shi, Z.Q., Gianolla, P., Huang, X.T., Preto, N., 2021. Onset of sedimentation near the Carnian/Norian boundary in the northwestern Sichuan Basin: New evidence from ammonoid biostratigraphy and zircon U-Pb geochronology. Palaeogeogr. Palaeoclimatol. Palaeoecol. 567, 110246.
Mu, H.X., Yan, D.P., Qiu, L., Yang, W.X., Kong, R.Y., Gong, L.X., Li, S.B., 2019. Formation of the Late Triassic western Sichuan foreland basin of the Qinling Orogenic Belt, SW China: Sedimentary and geochronological constraints from the Xujiahe Formation. J. Asian Earth Sci. 183, 103938.
Nesbitt, S.J., Sidor, C.A., Irmis, R.B., Angielczyk, K.D., Smith, R.M.H., Tsuji, L.A., 2010. Ecologically distinct dinosaurian sister group shows early diversification of Ornithodira. Nature 464, 95–98.
Nesbitt, S.J., Barrett, P.M., Werning, S., Sidor, C.A., Charig, A.J., 2013. The oldest dinosaur? A Middle Triassic dinosauriform from Tanzania. Biol. Lett. 9, 20120949.
Niedźwiedzki, G., 2005. Nowe znalezisko śladów dinozaurów w górnym triasie Tatr. Przegląd Gelologiczny 53, 410-413 (in Polish with English summary).
Niedźwiedzki, G., 2011. A Late Triassic dinosaur-dominated ichnofauna from the Tomanová Formation of the Tatra Mountains, central Europe. Acta Palaeontol. Pol. 56, 291–300.
Olsen, P.E., 1988. Paleontology and paleoecology of the Newark Supergroup (Early Mesozoic, eastern North America). In: Manspeizer, W. (Ed.), TriAssic-JurAssic Rifting: ContinentAl BreAkup And the Origin of the AtlAntic OceAn And PAssive MArgins, PArt A. Elsevier, Amsterdam, pp. 185–230.
Olsen, P.E., Huber, P., 1998. The oldest Late Triassic footprint assemblage from North America (Pekin Formation, Deep River Basin, North Carolina, USA). Southeast. Geol. 38, 77–90.
Olsen, P.E., Smith, J.B., McDonald, N.G., 1998. Type material of the type species of the classic theropod footprint genera *Eubrontes*, *Anchisauripus* and *Grallator* (Early Jurassic, Hartford and Deerfield basins, Connecticut and Massachusetts, USA). J. Vertebr. Paleontol. 18, 586–601.
Olsen, P.E., Sha, J.G., Fang, Y.N., Chang, C., Whiteside, J.H., Kinney, S., Sues, H.D., Kent, D., Schaller, M., Vajda, V., 2022. Arctic ice and the ecological rise of the dinosaurs. Sci. Adv. 8 (26), 1–9. https://doi.org/10.1126/sciadv.abo6342.
Paton, C., Woodhead, J.D., Hellstrom, J.C., Hergt, J.M., Greig, A., Maas, R., 2010. Improved laser ablation U-Pb zircon geochronology through robust downhole fractionation correction. Geochem. Geophys. Geosyst. 11, Q0AA06.
Ran, B., Liu, S.G., Li, Z.W., Dong, J., Wang, Z.J., Ye, Y.H., Tian, Q., Huang, R., He, L., 2016. Chronology of the pyroclastic layer from Xujiahe Formation in the western Sichuan Basin and its geological significance. J. Chengdu Univ. Technol. (Sci. Technol. Ed.) 43, 727-736 (in Chinese with English abstract).
Rauhut, O.W.M., Hungerbühler, A., 2000. A review of European Triassic tetrapods. Gaia 15, 75–88.
Schaller, M.F., Wright, J.D., Kent, D.V., 2015. A 30 Myr record of Late Triassic atmospheric pCO_2 variation reflects a fundamental control of the carbon cycles by changes in continental weathering. Geol. Soc. America 127, 661–671.
Scotese, C.R., 2014. Atlas of Middle & Late Permian and Triassic paleogeographic maps. Map 44, Volume 3 of the PALEOMAP Atlas for ArcGIS, Mollweide Projection, PALEOMAP Project, Evanston, IL.
Sereno, P.C., 2012. Preface. J. Vertebrate Palaeontol. 32, 1–9.
Shi, Z.Q., Preto, N., Jiang, H.S., Krystyn, L., Zhang, Y., Ogg, J.G., Jin, X., Yuan, J.L., Yang, X.K., Du, Y.X., 2017. Demise of Late Triassic sponge mounds along the northwestern margin of the Yangtze Block, South China: Related to the Carnian Pluvial Phase?. Palaeogeogr. Palaeoclimatol. Palaeoecol. 474, 247–263.
Sun, Y.D., Orchard, M.J., Kocsis, Á.T., Joachimski, M.M., 2020. Carnian-Norian (Late Triassic) climate change: Evidence from conodont oxygen isotope thermometry with implications for reef development and Wrangellian tectonics. Earth Planet. Sci. Lett. 534, 116082.
Tian, N., Wang, Y.D., Philippe, M., Li, L.Q., Xie, X.P., Jiang, Z.K., 2016. New record of fossil wood *Xenoxylon* from the Late Triassic in the Sichuan Basin, southern China and its paleoclimatic implications. Palaeogeogr. Palaeoclimatol. Palaeoecol. 464, 65–75.
Trotter, J.A., Williams, I.S., Nicora, A., Mazza, M., Rigo, M., 2015. Long-term cycles of Triassic climate change: a new $\delta^{18}O$ record from conodont apatite. Earth Planet. Sci. Lett. 415, 165–174.
Wang, Y.D., Fu, B.H., Xie, X.P., Huang, Q.S., Li, K., Li, G., Liu, Z.S., Yu, J.X., Pan, Y.H., Tian, N., Jiang, Z.K., 2010. The terrestrial Triassic and Jurassic systems in the Sichuan Basin, China. University of Science and Technology of China Press, p. 109 (in Chinese with English abstract).
Wang, Q.W., Kan, Z.Z., Liang, B., Cai, K.J., 2005. Discovery of track fossils of dinosaurs in Late Triassic strata of Tianquan, Sichuan, China. Geol. Bull. China 24, 1179-1180 (in Chinese with English abstract).
Wang, B.P., Li, J.J., Bai, Z.Q., Gao, J.M., Dong, S.R., Hu, B.L., Zhao, S.Q., Chang, J.Q., 2016. Research on dinosaur footprints in Zhizhou, Shaanxi Province, China. Acta Geol. Sin. 90, 1–18.
Wang, X.J., Wang, C.Y., Chen, X.E., Liu, S., Fan, Y.N., Lin, R.N., 2021. Stratigraphic correlation of the Upper Triassic and its sedimentary filling characteristics in the western and central Sichuan Basin. Acta Sedimentol. Sin.. https://doi.org/10.14027/j.issn.1000-0550.2021.087 (in Chinese with English abstract).
Weems, R.E., 2003. *Plateosaurus* foot structure suggests a single trackmaker for *Eubrontes* and *Gigandipus* footprints. In: LeTourneau, P.M., Olsen, P.E. (Eds.), 2003. The great rift valleys of Pangea in eastern North America, volume 2. Columbia University Press, New York, pp. 293–313.
Welles, S.P., 1971. Dinosaur footprints from the Kayenta Formation of northern Arizona. Plateau 44, 27–38.
Whiteside, J.H., Lindström, S., Irmis, R.B., Glasspool, I.J., Schaller, M.F., Dunlavey, M., Nesbitt, S.J., Smith, N.D., Turner, A.H., 2015. Extreme ecosystem instability suppressed tropical dinosaur dominance for 30 million years. Proceedings of the National Academy of Sciences USA 112, 7909-7913.
Wu, Y.B., Zheng, Y.F., 2013. Tectonic evolution of a composite collision orogen: An overview on the Qinling-Tongbai-Hong'an-Dabie-Sulu orogenic belt in central China. Gondw. Res. 23, 1402–1428.
Xing, L.D., Ba, J., Lockley, M.G., Klein, H., Yan, S.W., Romilio, A., Chou, C.Y., Persons IV, W.S., 2018. Late Triassic sauropodomorph and Middle Jurassic theropod tracks from the Xichang Basin, Sichuan Province, southwestern China: First report of the ichnogenus *Carmelopodus*. J. Palaeogeogr. 7, 1-13.
Xing, L.D., Klein, H., Lockley, M.G., Wang, S.L., Chen, W., Ye, Y., Matsukawa, M., Zhang, J.P., 2013a. Earliest records of theropod and mammal-like tetrapod footprints in the Upper Triassic of Sichuan Basin, China. Vertebrata Palasiatica 51, 184–198.
Xing, L.D., Klein, H., Lockley, M.G., Li, J.J., Zhang, J.P., Matsukawa, M., Xiao, J.F., 2013b. *Chirotherium* trackways from the Middle Triassic of Guizhou, China. Ichnos 20, 99–107.
Xing, L.D., Klein, H., Lockley, M.G., Kan, Z.Z., Zhang, J.J., Peng, G.Z., Ye, Y., 2014a. First chirothere and possible grallatorid footprint assemblage from the Upper Triassic Baoding Formation of Sichuan Province, southwestern China. Palaeogeogr. Palaeoclimatol. Palaeoecol. 412, 169–176.
Xing, L.D., Peng, G.Z., Marty, D., Ye, Y., Klein, H., Li, J.J., Gierliński, G.D., Shu, C.K., 2014b. An unusual trackway of a possibly bipedal archosaur from the Late Triassic of the Sichuan Basin, China. Acta Palaeontol. Pol. 59, 863–871.
Xu, Y.Y., Popa, M.E., Zhang, T.S., Lu, N., Zeng, J.L., Zhang, X.Q., Li, L.Q., Wang, Y.D., 2021. Re-appraisal of *Anthrophyopsis* (Gymnospermae): New material from China and global fossil records. Rev. Palaeobot. Palynol. 292, 104475.
Xu, Z.H., Wang, Z.C., Hu, S.Y., Zhu, S.F., Jiang, Q.C., 2010. Paleoclimate during depositional period of the Upper Triassic Xujiahe Formation in Sichuan Basin. J. Palaeogeogr. 12, 415-424 (in Chinese with English abstract).
Yang, X.L., Yang, D.H., 1987. Dinosaur footprints of Sichuan Basin. Sichuan Science and Technology Publications, Chengdu, pp. 1–30 (in Chinese).
Yang, W., Zuo, R.S., Chen, D.X., Jiang, Z.X., Guo, L.S., Liu, Z.Y., Chen, R., Zhang, Y.P., Zhang, Z.Y., Song, Y., Luo, Q., Wang, Q.Y., Wang, J.B., Chen, L., Li, Y.H., Zhang, C., 2019. Climate and tectonic-driven deposition of sandwiched continental shale units: New insights from petrology, geochemistry, and integrated provenance analyses (the western Sichuan subsiding Basin, Southwest China). Int. J. Coal Geol. 211, 103227.
Yates, A.M., 2007. The first complete skull of the Triassic dinosaur *Melanorosaurus* Haughton (Sauropodomorpha: Anchisauria). Spec. Pap. Palaeontol. 77, 9–55.
Zhang, Y., Jia, D., Shen, L., Yin, H.W., Chen, Z.X., Li, H.B., Li, Z.G., Sun, C., 2015. Provenance of detrital zircons in the Late Triassic Sichuan foreland basin: constraints on the evolution of the Qinling Orogen and Longmen Shan thrust-fold belt in central China. Int. Geol. Rev. 57, 1806–1824.
Zhu, M., Chen, H.L., Zhou, J., Yang, S.F., 2017. Provenance change from the Middle to Late Triassic of the southwestern Sichuan basin, Southwest China: Constraints from the sedimentary record and its tectonic significance. Tectonophysics 700–701, 92–107.